Advances in Polymer Technology

Advanced Polymers and Related Composite Materials for Energy Technology

Lead Guest Editor: Jian Hou
Guest Editors: Hai Chang Zhang, Xian-Ru He, and Weixia Zhang

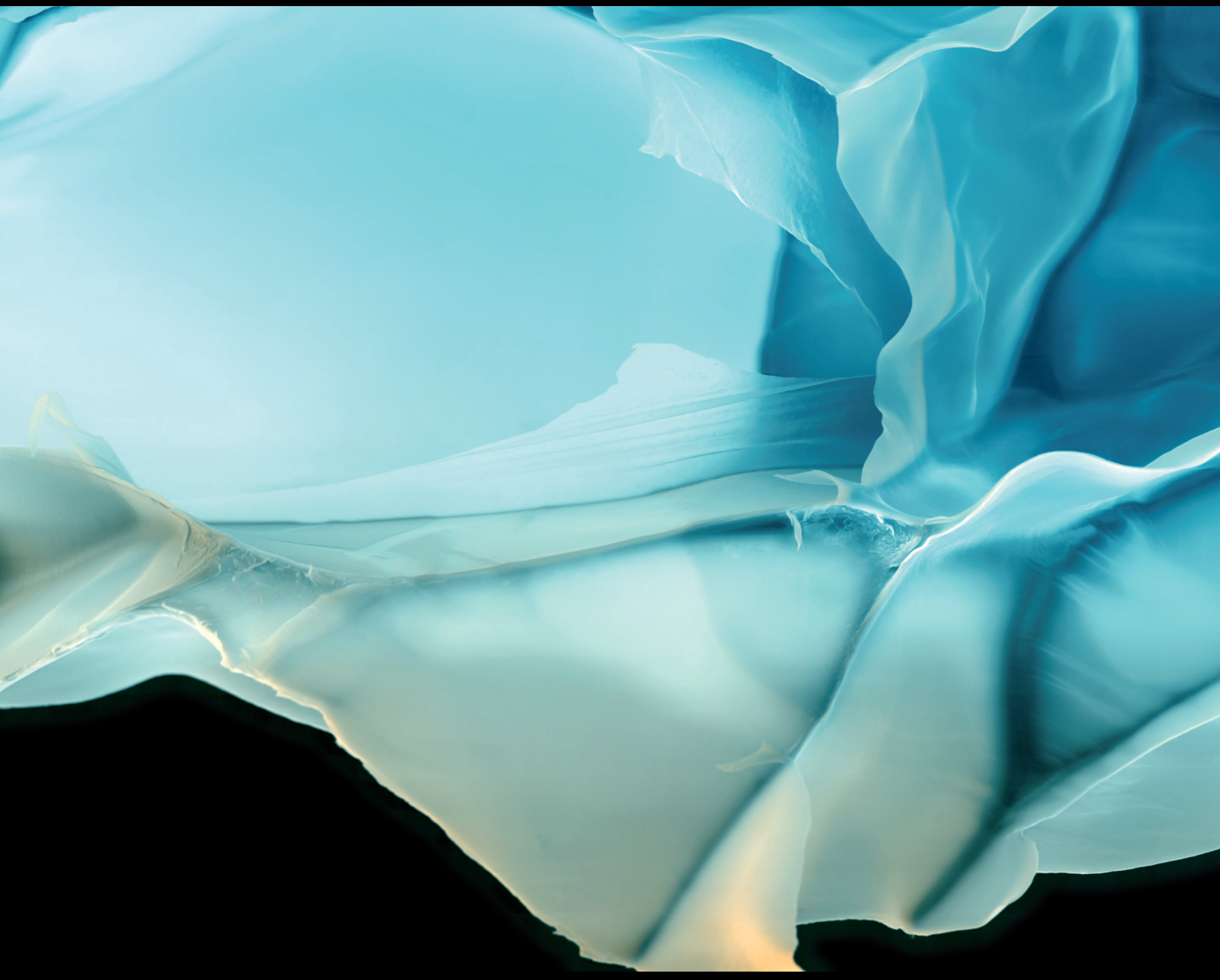

Advanced Polymers and Related Composite Materials for Energy Technology

Advances in Polymer Technology

Advanced Polymers and Related Composite Materials for Energy Technology

Lead Guest Editor: Jian Hou
Guest Editors: Hai Chang Zhang, Xian-Ru He, and Weixia Zhang

Contents

Numerical Simulation and Experimental Study on Flow of Polymer Aqueous Solution in Porous Jet Nozzle
Minghui Wei, Chenghuai Wu, and Yanxi Zhou
Research Article (9 pages), Article ID 7580460, Volume 2020 (2020)

Study on Wellbore Temperature and Pressure Distribution in Process of Gas Hydrate Mined by Polymer Additive CO_2 Jet
Minghui Wei, Chenghuai Wu, and Yanxi Zhou
Research Article (7 pages), Article ID 2914375, Volume 2020 (2020)

Hindawi
Advances in Polymer Technology
Volume 2020, Article ID 7580460, 9 pages
https://doi.org/10.1155/2020/7580460

Research Article

Numerical Simulation and Experimental Study on Flow of Polymer Aqueous Solution in Porous Jet Nozzle

Minghui Wei, Chenghuai Wu, and Yanxi Zhou

College of Mechanical and Electrical Engineering, Southwest Petroleum University, Chengdu, China

Correspondence should be addressed to Minghui Wei; wmh881988@163.com

Received 30 August 2019; Accepted 9 March 2020; Published 26 March 2020

Academic Editor: Gyorgy Szekely

The addition of a polymer to the jet medium enhances its ability to break rock, and the structure of the nozzle plays a vital role in the full utilization of energy. In this paper, a self-propelled porous jet bit with a support plate is designed, which can prevent the drill bit from jamming due to the jet nozzle against the bottom of the well during the drilling process. And the structural design of the cone-converging nozzle is applied to the forward center nozzle. The polymer additive jet flow field and the pure water jet flow field were compared by numerical simulation and experimental investigation. The results show that the polymer additive jet has a longer isokinetic core, and the rock-breaking volume of the polymer additive jet is much larger than that of the pure water jet, and the optimal spray distance is increased. The forward central jet with the conical convergent nozzle structure has more efficient rock-breaking ability.

1. Introduction

High-pressure water jet technology is widely used in cutting, crushing, cleaning, and other aspects due to its high material utilization, no thermal effect, concentrated energy, safe operation, and no dust generation. The factors affecting the impact of the water jet are mainly the nozzle structure, the driving force of the jet, the nature of the jet liquid, the spray distance, and so on. The addition of high molecular weight polymer to the jet can effectively reduce the resistance of the fluid, reduce the energy consumption, and improve the isokinetic core of the jet. It was first proposed by Rosler and Bankoff [1]. Li et al. [2] and others added high polymer additives to the jet-breaking rock for experimental research. Studies have shown that, under the same conditions, the rock-breaking volume of the dilute solution jet of polyacrylamide (PAM) is about twice the volume of the pure water jet-breaking rock, and the jetting distance of the largest rock-breaking efficiency is larger than that of the pure water jet. Liu and Li [3, 4] of China University of Petroleum measured the flow field of the pure water jet and different concentration additive (PAM) jets through LDV. The experimental results show that the additive jet is longer than the constant velocity core of the pure water jet, and the constant velocity core is the longest when the additive concentration is in the range of 100–200 mg/L. Wang et al. [5–7] used the test method to study the axial dynamic pressure distribution of the polymer additive jet in the submerged state. The results show that the polymer additive can reduce the energy loss of the fluid in the pipeline and at the nozzle, increase the velocity and dynamic pressure of the jet at the nozzle outlet, and increase the constant velocity core of the circular jet. The results of the rock-breaking test show that the polymer additive can improve the rock-breaking ability of the jet. Yang et al. [8–11] used PIV velocimetry to study the abrasive slurry jet under submerged conditions and systematically measured the relationship between the velocity of the fluid and abrasive and the concentration of PAM. It is found that, as the concentration of the polymer in the drilling fluid increases, the velocity of the fluid in the jet and the velocity of the abrasive particles increase correspondingly, and as the concentration of the polymer increases, the convergence of the jet increases. Polyacrylamide has the effect of suppressing the lateral expansion of the jet and reducing the axial attenuation of the jet. However, there are few simulation analyses of the

additive jet flow field at present, and most of the research studies tend to be experimental research on the effects of actual cutting and crushing [12–19]. Therefore, it is important to strengthen the flow field study of polymer additive jets.

Radial horizontal well technology began in the 1980s. In the past 20 years, radial horizontal well technology has developed rapidly and has the potential to develop unconventional oil and gas [20–24]. This technology requires the use of the high-efficiency rock-breaking water jet bit, high-pressure fluid through small diameter coiled tubing, and high-pressure hose into the jet bit in order to achieve rock-breaking drilling effect. In this case, jet bit is an indispensable technology, which not only needs to break rocks and enlarge holes but also needs to provide traction for the high-pressure hose [25–28]. However, in the actual drilling process, due to the complicated conditions at the bottom of the well, the forward nozzle of the drill bit often contacts with the hard rock layer to be drilled directly. In addition, the forward thrust applied to the nozzle after drilling leads to the forward nozzle being firmly blocked by the rock layer, which is the phenomenon of "stuck" of the water jet bit.

In order to solve the above problems, this paper designs a self-entering multihole jet bit with the support plate. At the same time, the structural design of the conical convergent nozzle is applied to the forward center hole to increase the equal velocity core length to improve the rock-breaking efficiency [29–32]. The flow field of the jet bit is analyzed by the numerical simulation method, and the influence of the support plate on the drilling of the water jet bit and the influence of diffuse flow chip removal are studied. In order to protect oil and gas reservoirs and effectively carry rocks, it is better to add a certain amount of polymer additives in the jet medium, and the jet effect will be different from that of the pure water jet. Through the numerical simulation analysis of the polymer additive jet flow field and pure water jet flow field, the influence of polymer additive on jet rock-breaking effect is explored. The research results can guide the hydraulic parameter design of horizontal drilling.

2. Nozzle Structure

As shown in Figure 1, the most important feature of the self-propelled porous jet bit with the support plate is that the front part of the bit has the support plate, which is used to maintain a certain distance between the bit and the drilling bottom to prevent the water jet bit from jamming during drilling. The forward nozzle is distributed in a structure of 1 + 3, that is, one central nozzle and three nozzles distributed in the same circle around the central hole at the same angle. And the fluid ejected will eventually form the perforation with area connectivity within a certain diameter range. Moreover, the structural design of the conical convergent nozzle is applied to the central nozzle, which can minimize the diffusion angle of jet flows, and the higher the density of jet flows, the more concentrated the energy [33]. The structural parameters of the bit mainly include the length of the bit $L_1 = 40$ mm, the outer diameter $D_1 = 18$ mm, the inner diameter $D_2 = 10$ mm, the support plate length $L_2 = 10$ mm, the diameter of the forward circular and backward holes $D_1 = 1$ mm, the back hole diffusion angle $\alpha_2 = 30^\circ$, the diameter of the front central hole $D_2 = 1$ mm, the forward hole diffusion angle $\alpha_3 = 15^\circ$, and the front central hole cone $\alpha_1 = 13.5^\circ$.

Figure 2 is the geometric model of a self-entering porous jet bit with the support plate established by SoildWorks, 3D modeling software. In this paper, a comparative analysis of the polymer additive jet flow field and pure water jet flow field will be built on this model.

3. Numerical Simulation Model and Boundary Conditions

3.1. Control Equation. The research object in this paper is the flow field under the nonsubmerged jet, and there is no violent vortex movement due to the high flow velocity of the polymer additive generated by the self-entering porous jet bit and the area of high Reynolds number inside and outside the bit. The standard k-ε turbulence model is more suitable for complete turbulence. The transport equation for the standard k-ε cycle turbulence model is as follows [34]:

$$\frac{\partial(\rho k)}{\partial t} + \frac{\partial(\rho k u_i)}{\partial x_i} = \frac{\partial}{\partial x_j}\left[\left(\mu + \frac{\mu_t}{\sigma_k}\right)\frac{\partial k}{\partial x_j}\right] + G_k + G_b - \rho\varepsilon - Y_M + S_k, \tag{1}$$

$$\frac{\partial(\rho \varepsilon)}{\partial t} + \frac{\partial(\rho \varepsilon u_i)}{\partial x_i} = \frac{\partial}{\partial x_j}\left[\left(\mu + \frac{\mu_t}{\sigma_\varepsilon}\right)\frac{\partial \varepsilon}{\partial x_j}\right] + G_{1\varepsilon}\frac{\varepsilon}{k}\left(G_k + G_{3\varepsilon}G_b\right) - G_{2\varepsilon}\rho\frac{\varepsilon^2}{k} + S_\varepsilon, \tag{2}$$

where

$$\begin{cases} G_k = \mu_t\left(\dfrac{\partial u_i}{\partial x_j} + \dfrac{\partial u_j}{\partial x_i}\right)\dfrac{\partial u_i}{\partial x_j} \\ G_b = \beta g_i \dfrac{\mu_t}{\mathrm{Pr}_t}\dfrac{\partial T}{\partial x_i}, \\ \beta = -\dfrac{1}{\rho}\dfrac{\partial \rho}{\partial T}, \\ Y_M = 2\rho\varepsilon M_t^2, \\ M_t = \sqrt{\dfrac{k}{a^2}}, \\ a = \sqrt{\gamma R T}, \end{cases} \tag{3}$$

where G_k is the turbulent kinetic energy generated by the average velocity gradient, G_b is generated by the turbulent

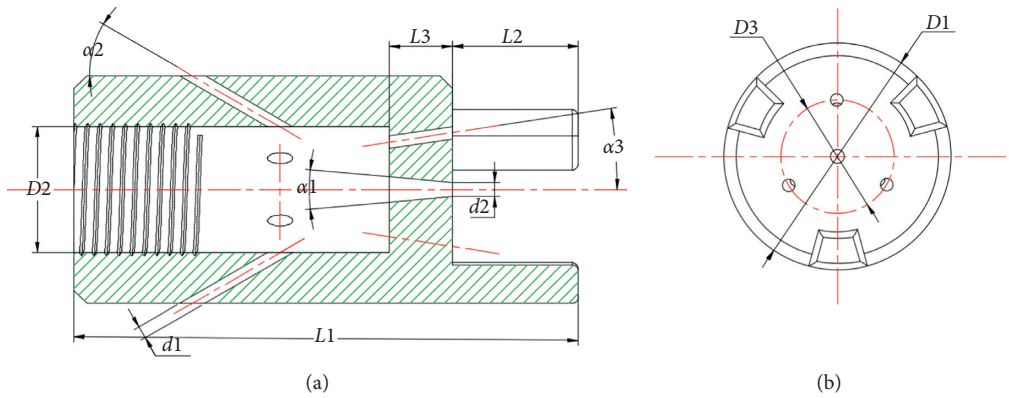

Figure 1: Structure diagram of the self-propelled multihole jet bit with the support plate.

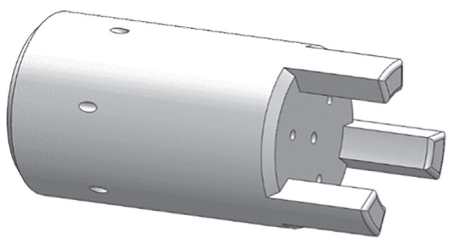

Figure 2: Geometric model.

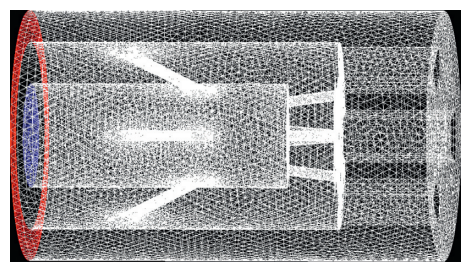

Figure 3: Grid division of the computing domain.

kinetic energy caused by buoyancy, and Y_M is the influence of compressible turbulence pulsation expansion on the total dissipation rate. $C_{1\varepsilon}$, $C_{2\varepsilon}$, and $C_{3\varepsilon}$ are the empirical constants of the standard k-ε turbulence model, and the default values in FLUENT are $C_{1\varepsilon} = 1.44$, $C_{2\varepsilon} = 1.92$, and $C_{3\varepsilon} = 0.09$. The readings for σ_k and σ_ε are the Puente numbers corresponding to the turbulence kinetic energy and turbulence dissipation rate, respectively. The default values for FLUENT are $\sigma_k = 1.0$ and $\sigma_\varepsilon = 1.3$. Pr_t is the Prandtl number of turbulence, and $\mathrm{P}r_t = 0.85$ by default. g_i is the component of gravitational acceleration in the direction of i; β is the coefficient of thermal expansion; M_t is the turbulent Mach number; and a is the speed of sound.

3.2. Meshing. As shown in Figure 3, it is a schematic diagram of mesh division of the three-dimensional model of the fluid domain. This model adopts the nonuniform mesh size, so as to capture the small features in the model. The left part of the grid model is the fluid inlet boundary, and the red part is the fluid outlet boundary. The mesh is much finer when the flow field gradient is large, such as the nozzle outlet and the bottom wall. MESHING module in ANSYS has the function of grid quality inspection. The highest, lowest, and average mass index of the grid divided by this model is 0.99955, 0.38299, and 0.87799. Generally speaking, if the mesh quality is higher than 0.8, it is considered as good mesh and can complete simulation tasks with high quality.

3.3. Boundary Conditions. Inlet boundary: the inlet boundary of absolute velocity is adopted, the velocity direction is the normal direction of the inlet, the absolute velocity of the inlet is 15 m/s, and the radial velocity is 0 m/s.

Outlet boundary: both forward and backward outlet pressure adopt environmental pressure. Static pressure $P_s = 0.2$ MPa.

Wall condition: the solid wall boundary without slip adiabatic is adopted, and the particles will bounce back into the calculation domain after hitting the wall.

3.4. Material Setting. The simulated jet medium was water solution of pure water and polyacrylamide (PAM), and the material of the pure water jet was set as 1 g/cm^3 with a viscosity of 0.85 Pa·s. The polymer additive jet has a customized fluid density of 1.5 g/cm^3 and viscosity of 0.39 Pa·s [35]. In this paper, when comparing the flow fields of the two jets, only the material settings are different, and the others all use the same settings.

4. Numerical Simulation Calculation Results and Analysis

4.1. Comparison of Flow Field Characteristics between Pure Water Jet and Polymer Additive Jet. The flow profile of the pure water jet and the polymer additive jet in the cross section of the bit center axis is shown in Figure 4. On the left is the velocity distribution cloud diagram of the polymer additive jet, and on the right is the velocity distribution cloud diagram of the pure water jet. The two fluids are ejected at high speed through the forward and backward holes of the drill bit, wherein the fluid ejected through the forward hole mainly breaks the rock. The effect of the fluid ejected

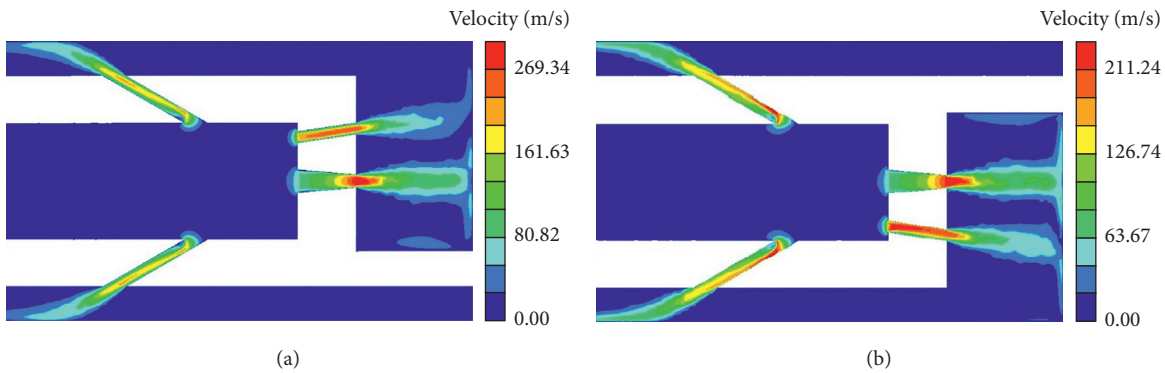

Figure 4: Velocity cloud diagram of cross section of two kinds of fluid in the center axis of the jet bit.

through the rear hole is mainly to ream the hole and provide the self-feeding force of the drill bit. Under the same conditions, the two jet decay laws are similar, and the difference is the polymer additive jet at the nozzle exit speed is much larger. The reason is that the interaction between the pure water jet and the surrounding stationary fluid is larger and the velocity attenuation is serious.

Therefore, under the same pump pressure, polymer additive jet has better rock-breaking effect than the water jet. That is to say, adding polymer to water can improve the efficiency of rock breaking.

4.2. Velocity Distribution of the Forward Jet. Figure 5 shows the cloud diagram of velocity distribution of the polymer additive jet in the forward jet of the drill bit. The section shown in the figure includes a circular hole, a central hole, and a support plate. The cone angle design of the central hole forms a smaller jet diffusion angle, which makes the jet more dense and the more concentrated the energy. It can be clearly seen from the figure that the central hole designed by cone angle has longer jet isokinetic core than other circular common holes and has greater impact force and better rock-breaking effect than other circumferential hole jets. Therefore, the forward central hole plays a major role in rock breaking. Since the other three holes with the same circular distribution are at a certain angle with the central axis of the drill bit, the jet flow formed by the three holes with the same circular distribution will have a certain shear force when hitting the rock, and such shear force is also conducive to rock breaking.

4.3. Velocity Distribution of the Backward Jet. The flow pattern of the backward orifice jet velocity distribution of the self-propelled porous jet drill bit is shown in Figure 6. There are a total of six backward orifices, which are evenly distributed on the same circumference. Part of the fluid enters into the nozzle and jets to the annulus from the inside of the drill bit, forming a backward jet flow. The maximum velocity of the fluid at the outlet of the backward orifice reaches 203.2 m/s. Under the influence of the surrounding fluid confining pressure, the velocity of the backward jet dissipates somewhat. When the jet finally impacts the rock, the impact

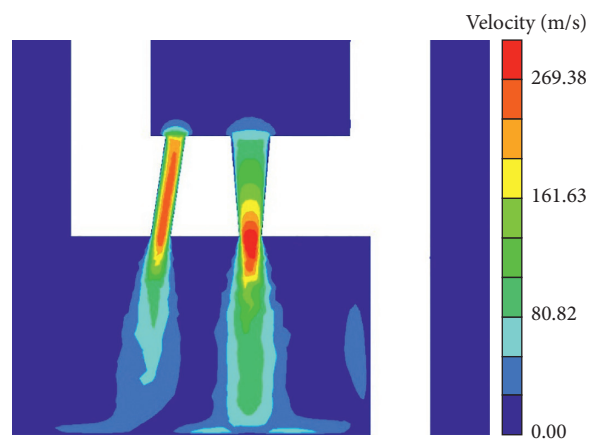

Figure 5: Forward jet velocity cloud diagram of the jet bit.

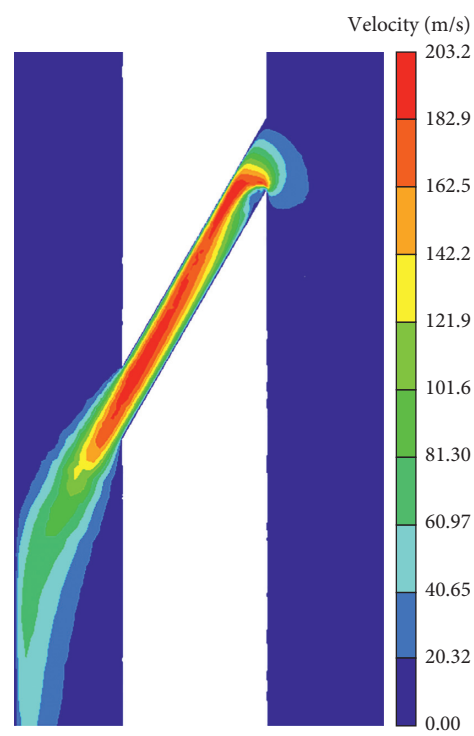

Figure 6: Backward jet velocity cloud diagram of the jet bit.

velocity is still as high as 101.6 m/s, and the high-speed fluid generates strong shear stress on the wall of the hole, making it more conducive to expanding the aperture of the broken rock.

In addition, the strong propulsive force generated by the backward jet of the polymer additive forms the main driving force for the bit to realize self-propulsion. Due to the viscosity of the polymer additive solution, the cuttings generated at the bottom of the well are more easily discharged through the backward jet.

4.4. Downhole Flow Field Analysis

4.4.1. Velocity Distribution. As shown in Figure 7, after the jet of the polymer additive impinges on the bottom hole, the jet fluid flows radially along the bottom hole under the restriction of the bottom hole, forming a diffuse flow with high speed along the bottom hole. This layer of diffuse flow from the polymer additive solution drives the cuttings at the bottom of the well to move laterally together to achieve timely cutting removal.

The research shows that when the wellbore boundary condition is no slip wall surface, the maximum diffuse flow velocity appears within the height range of 0.5 mm from the wellbore bottom, and the maximum diffuse flow velocity value can reach 50% to 80% of the exit velocity of the jet nozzle. A section, 0.5 mm, from the bottom of the well is taken as the research object, and the velocity distribution cloud diagram of the flow field in this section is shown in Figure 8. It can be seen from the figure that four circular high-speed regions are distributed in the velocity distribution cloud map, which is the cross section of the jet formed by the forward jet. In addition, the flow velocity of the jet formed by the forward central nozzle at the bottom of the well is obviously greater, and the crushing depth will also be deeper. The three white areas in the figure are the zero velocity areas formed by the support plate. The staggered arrangement with the other three nozzles with the same circular distribution is to reduce the influence of the support plate on the jet flow. Moreover, the fluid flow velocity around the circular arc surface of the support plate is high, and the crushed rock debris does not accumulate on the inner circular arc surface of the support plate, so as to timely clean the bottom rock cuttings.

Figure 9 shows the cloud diagram of the velocity distribution at the bottom of the well of the pure water jet. It can be seen from the figure that the velocity distribution at the bottom of the well of the pure water jet is roughly the same as that of the polymer additive jet, but the corresponding velocity is much smaller. The maximum impact velocity of the pure water jet hitting the bottom of the well is about 95 m/s, but the maximum impact velocity of the jet with polymer added can reach 106 m/s. This proves that the polymer additive jet has better rock-breaking effect.

4.4.2. Pressure Distribution. Figure 10 shows the cloud diagram of static pressure distribution at the bottom of the well of the polymer additive jet. Compared with other three holes

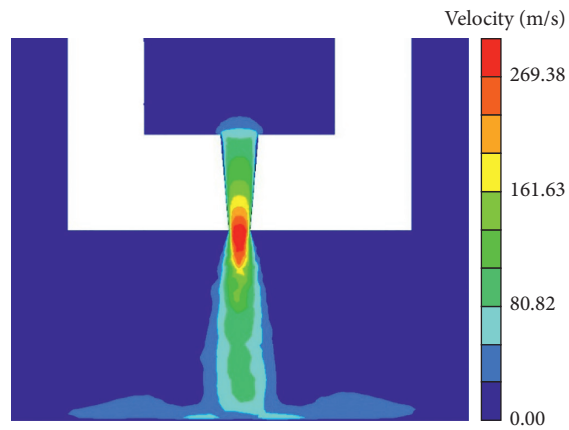

Figure 7: Backward jet velocity cloud diagram of the jet bit.

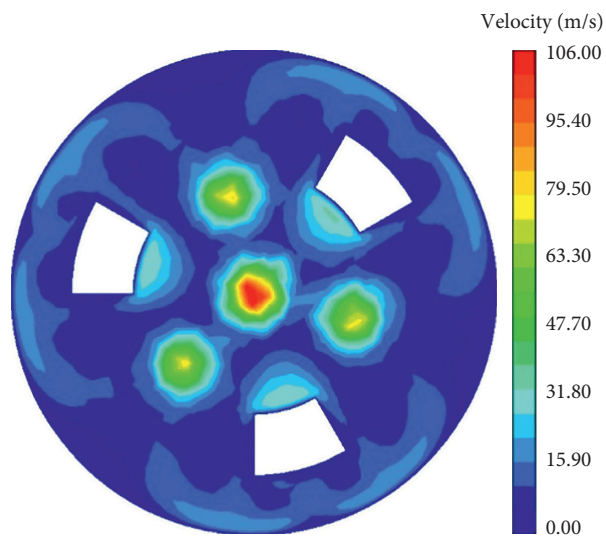

Figure 8: Bottom hole velocity distribution cloud image of the polymer additive jet.

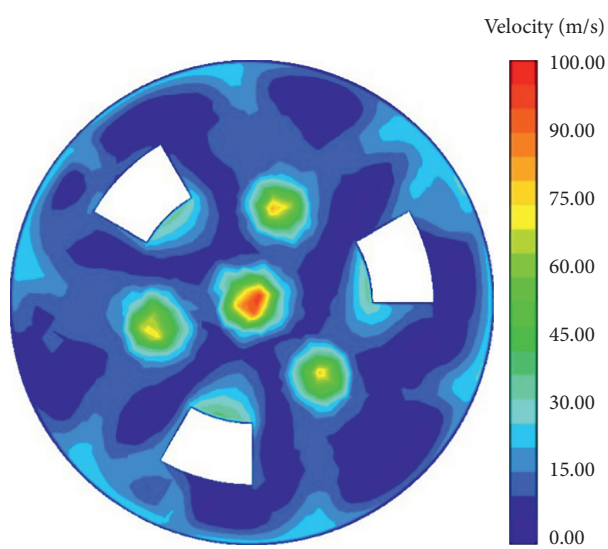

Figure 9: Bottom hole velocity distribution cloud image of the pure water jet.

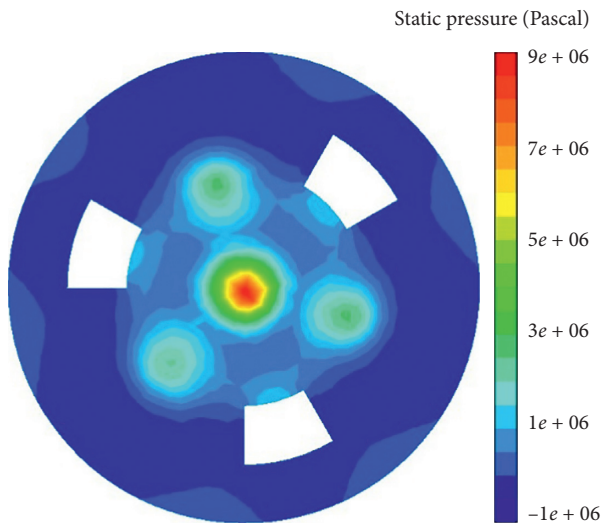

Figure 10: Bottom hole static pressure distribution cloud image of the polymer additive jet.

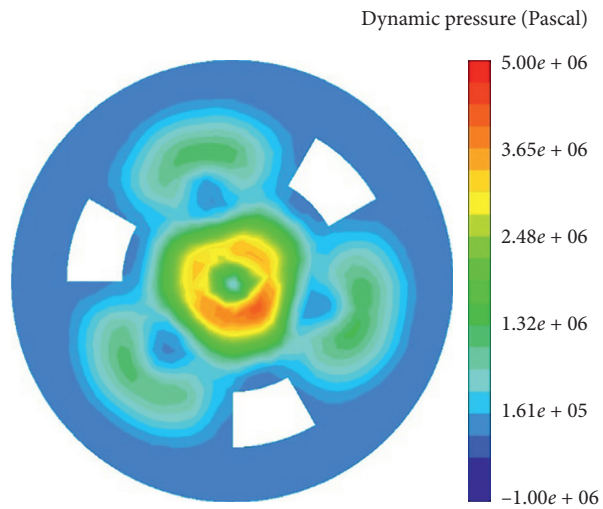

Figure 11: Bottom hole dynamic pressure distribution cloud image of the polymer additive jet.

with the same circular distribution, the static pressure of the jet formed by the forward central hole is much larger. The jet static pressure formed by the central hole is at most about 9 MPa, while the jet static pressure formed by the holes with the same circular distribution is at most about 4 MPa. And all the static pressure areas formed showed a decreasing trend from the center to the surrounding area.

Figure 11 shows the cloud diagram of the bottom hole dynamic pressure distribution of the jet flow of the polymer additive. The dynamic pressure distribution is quite different from the static pressure distribution. The area where the jet impinges on the bottom of the well is the area with the minimum dynamic pressure, and the surrounding dynamic pressure gradually increases. When it is close to the wall of the well, the dynamic pressure gradually decreases.

5. Experimental

5.1. Material. The polymer used in the experiment is polyacrylamide (PAM), which is a water-soluble linear polymer synthesized with a high degree of polymerization. PAM density is 1.32 g/cm^3. Because PAM has stronger shear resistance than other polymers and is easily soluble in water, it is particularly suitable for fluid conveying systems with high shear local resistance elements. The molecular weight of PAM used in this experiment is over 10 million, bought in China Xinqi chemical plant, located in Heluo Town, Gongyi City, Henan Province.

5.2. Sample Preparation. Wang et al. [5–7] showed that, with the increase of additive concentration, the crushing depth of the rock first increased and then decreased, and there was an optimal concentration of the polymer additive, so the concentration of the additive was selected as 200 mg/L in this experiment. When preparing polymer additive aqueous solution, first 5000 mg/L high concentration aqueous solution is prepared, and then 200 mg/L required concentration polymer additive solution is prepared, it is fully stirred (24 h) to make the additive mix evenly, and uniform jet properties are obtained, so as to ensure the maximum performance of the additive. Because the polymer chain of polyacrylamide in the polymer additive solution is easy to break during the impact process, in order to ensure the comparability of the experiment, the additive solution is used once in this experiment instead of repeated use.

5.3. Experimental Equipment. This experiment was carried out in Southwest Petroleum University, which mainly studied and compared the rock-breaking effect of the pure water jet and polymer additive jet. The experimental device is shown in Figure 12, including multistage pump, pipeline, throttle valve, water tank, pressure gauge, electronic flowmeter, water jet nozzle, and jet rock-breaking system. The jetting rock-breaking system can adjust the jetting distance freely. The highest pressure of the multistage pump can reach 40 MPa, and the volume of the water tank is 20 L. The rocks used in the experiment are natural sandstone. The experimental nozzle adopts a straight single-hole nozzle with a cone angle of 12.3°, with a nozzle outlet diameter of 4 mm, and with an outlet length of 10 mm.

5.4. Condition Setting. The two groups of experiments adopted the same injection pressure of 30 MPa, the same injection time of 60 s, and the same rock to be broken, with only difference in drilling fluid and spraying distance. The rock used in the experiment is natural sandstone, and the crushing effect is characterized by the volume of rock breaking by fixed time and fixed-point impact crushing. In order to make the experimental data accurate and reliable and reduce the influence of experimental error, the polymer additive jet experiment and pure water jet experiment were repeated three times, and the average value of the results of the three experiments was taken as the rock-breaking volume.

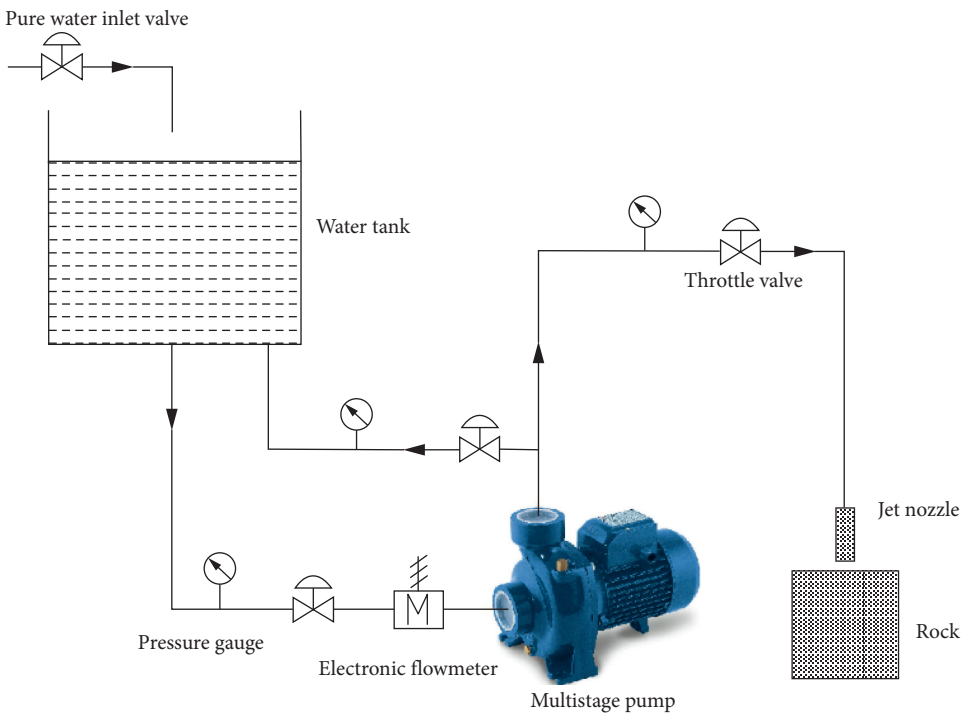

Figure 12: Schematic diagram of experimental equipment.

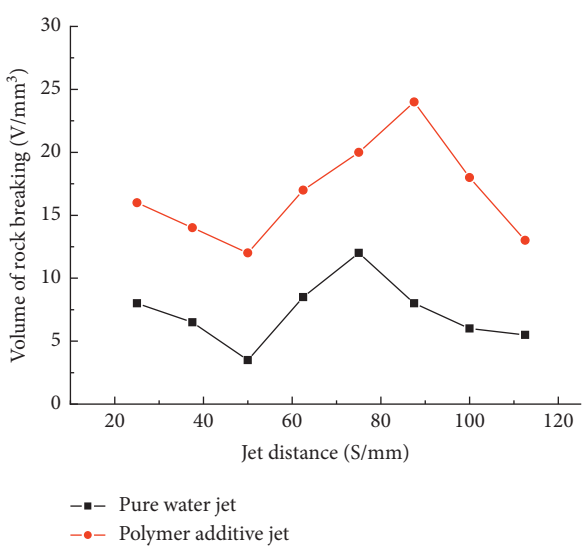

Figure 13: Comparison of rock-breaking effect between water jet and polymer additive jet.

5.5. Experimental Results. The experimental results are shown in Figure 13, which are the comparison curve of rock-breaking volume between the additive jet and water jet. It can be seen from the diagram that the rock-breaking effect of the pure water jet and polymer additive jet shows the trend of first decreasing and then increasing with the increase of spray distance. When the optimal spray distance is reached, the rock-breaking effect decreases with the increase of spray distance. In this experiment, the optimal spray distance of the pure water jet is 75.2 mm, while the optimal spray distance of the polymer additive is about 87.5 mm, and the optimal spray distance of the polymer additive jet increases 12.3 mm compared with that of the pure water jet. This indicates that the polymer additive increases the rock-breaking effect of the jet.

Before the spray distance of the two jets reaches the optimal spray distance, the trend of rock-breaking effect of the two jets varies with the spray distance which is approximately the same. However, when the spray distance of the two jets reached the optimal spray distance, the rock-breaking efficiency of the polymer additive jet decreased faster with the spray distance than that of the pure water jet.

Under the same conditions, the rock-breaking volume of the additive jet is about twice or more than that of the pure water jet. Moreover, the optimal spray distance of the additive jet is larger than that of the pure water jet. This is because the viscosity of the jet medium increases with the addition of polymer additives, which changes the structural characteristics of the jet. The axial velocity attenuation of the jet becomes slower, and the effective jetting distance of the jet increases. It shows that the polymer additive jet has more impact force and better rock-breaking effect. The experimental results are in good agreement with the numerical simulation results, indicating that the numerical simulation method is reliable in analyzing and designing the flow field characteristics of the jet bit.

6. Conclusions

Based on the above study, we can draw the following conclusions:

(1) In this paper, a self-propelled multihole jet bit with the support plate is designed, which can prevent the

drill bit from jamming due to the jet nozzle against the bottom of the well during the drilling process

(2) When the jet fluid uses the polymer additive solution, the rock-breaking volume of the polymer additive jet is about twice or more than that of the pure water jet, and its optimal jet distance will increase accordingly, which indicates that the polymer additive jet has more efficient rock-breaking efficiency

(3) It can be known from the bottom hole velocity distribution cloud chart and bottom hole pressure distribution cloud chart setup by polymer additive that the forward central nozzle designed by cone angle has more efficient rock-breaking efficiency and longer isovelocity core than other common nozzles with uniform distribution in circumference

Data Availability

All data included in this study are available upon request by contact with the corresponding author.

Conflicts of Interest

The authors declare that there are no conflicts of interest regarding the publication of this paper.

Acknowledgments

This research was funded by State Key Laboratory of Petroleum Resources and Prospecting, China University of Petroleum, Beijing, grant number PRP/open-1610 and the National Natural Science Foundation of China, grant number 51804267.

References

[1] R. S. Rosler and S. G. Bankoff, "Large-scale turbulence characteristics of a submerged water jet," *AIChE Journal*, vol. 9, no. 5, pp. 672–676, 1963.

[2] G. S. Li, C. Yi, J. L. Niu et al., "Experimental study on high polymer additive (super water) jet for rock erosion efficiency," *Oil Drilling Technology*, vol. 29, no. 6, Article ID 1001-0890, 2001.

[3] C. W. Liu and Z. M. Li, "Using LDV to study the flow field of polymer additive jets," in *Proceedings of the 1999 National Hydrodynamics Conference*, pp. 123–128, Beijing, China, 1999.

[4] Z. M. Li and C. W. Liu, "Experimental study on jet structure characteristics of polymer additive," *Drilling Fluid and Completion Fluid*, vol. 6, pp. 1–3, 1999.

[5] S. J. Wang, R. H. Wang, and Y. H. Bu, "Laboratory study on drilling by high molecular weight additive jetting," *Oil Driling & Production Technology*, vol. 21, no. 1, pp. 21–24, 1999.

[6] R. H. Wang, S. J. Wang, and Y. H. Bu, "Polymer additive jet structure characteristics," *Journal of China University of Petroleum (Edition of Natural Science)*, vol. 22, no. 1, pp. 38–40, 1998.

[7] S. J. Wang, R. H. Wang, and W. D. Zhou, "Influences of macromolecular additives on rotary-jet configuration characteristics," *Petroleum Drilling Techniques*, vol. 26, no. 3, pp. 55–62, 1998.

[8] Y. Y. Yang, Z. H. Shen, R. H. Wang et al., "Velocity profile of abrasive suspension swirling jet and influence of additive polyacrylamide," *Journal of China University of Petroleum (Edition of Natural Science)*, vol. 29, no. 1, pp. 34–36, 2005.

[9] Y. Y. Yang, R. H. Wang, Z. H. Shen et al., "Experimental study on velocity distribution of swirling jet with polyacry-lamide fluid," *Journal of China University of Petroleum (Edition of Natural Science)*, vol. 25, no. 6, pp. 38–41, 2001.

[10] Y. Y. Yang and G. S. Li, "Experimental study on ultra-high pressure abrasive jet breaking and cutting," *Petroleum Drilling Techniques*, vol. 3, no. 3, pp. 4-5, 2002.

[11] Y. Y. Yang, R. H. Wang, and W. D. Zhou, "Study on the effect of PAM on abrasive jet flow," *Petroleum Drilling Techniques*, vol. 29, no. 1, pp. 4–6, 2001.

[12] D. Feng, L. Shi, C. Guo, F. Wang, and Y. Chen, "Numerical and experimental study on the flow characteristics of abrasive slurry jet with polymer additives," *The International Journal of Advanced Manufacturing Technology*, vol. 95, no. 9–12, pp. 3289–3299, 2017.

[13] G. Seifert, R. Boing, X. L. Wu et al., "Additives are used to improve the effect of high pressure water jet in tunneling," *Colliery Mechanical & Electrical Technology*, vol. 5, no. 12, pp. 53–63, 1982.

[14] X. P. Jiang, S. G. Hu, and S. Y. Zhong, "An experimental study of abrasive water jet and improvement on the performance with high polymer drag reduction," *Journal of University of Shanghai for Science and Technology*, vol. 15, no. 2, pp. 87–91, 1993.

[15] H. N. Zuo, *Experimental Study on Adding Polymers in Abrasive Water Jet, Diss*, Hunan University of Technology, Xiangtan, China, 2013.

[16] J. H. Pei and Z. W. Bai, "Influence on cutting quality generated by high polymeric additives abrasive water jet," *Machine Tool & Hydraulics*, vol. 44, no. 15, pp. 142–146, 2016.

[17] J. H. Pei and D. Hu, "Experimental study on cutting taper by high polymeric additives abrasive water jet," *Manufacturing Technology & Machine Tool*, vol. 5, no. 34, pp. 83–86, 2016.

[18] J. H. Pei, Y. L. Wang, and J. H. Chen, "Theory and experiment to influences of macromolecular additives on jet cutting," *Journal of Lanzhou Petrochemical College of Technology*, vol. 16, no. 1, pp. 4–6, 2016.

[19] Y. Y. Zhang, X. C. Wang, and D. Hu, "Influence of adding a small amount high molecular polymer on cutting performance of abrasive water jet," *Journal of Sichuan University (Engineering Science Edition)*, vol. 46, no. 5, pp. 181–187, 2014.

[20] W. Dickinson and R. W. Dickinson, "Horizontal radial drilling system," in *Proceedings of the SPE California Regional Meeting*, Society of Petroleum Engineers, Bakersfield, CA, USA, March 1985.

[21] H. Y. Li, C. J. Wang, L. H. Shi et al., "Application and development of drilling and completion of the ultrashort-radius radial well by high pressure jet flow techniques," in *Proceedings of the International Oil and Gas Conference and Exhibition in China*, Beijing, China, November 2000.

[22] W. Dickinson, H. Dykstra, R. Nordlund et al., "Coiled-tubing radials placed by water-jet drilling: field results ,theory, and practice," in *Proceedings of the SPE Annual Technical Conference and Exhibition*, SPE, Houston, TX, USA, October 1993.

[23] C. W. Landers, "Method of and apparatus for horizontal well drilling," US Patent 6125949A, 2000.

[24] B. M. Henry, "Horizontal directional drilling in wells," US Patent 6889781B2, 2005.

[25] X. H. Zhu and W. Chen, "Analysis of influencing factors and parameter optimization of self-propelling force of self-propelling nozzle," *Research and Progress in Hydrodynamics*, vol. 33, no. 1, pp. 89–97, 2018.

[26] P. Buset, M. Riiber, A. Eek et al., "Jet drilling tool: cost-effective lateral drilling technology for enhanced oil recovery," in *Proceedings of the SPE/ICoTA Coiled Tubing Roundtable*, Society of Petroleum Engineers, Houston, TX, USA, March 2001.

[27] G. Bi, D. J. Ma, G. S. Li et al., "Hydraulic jet side tracking radial horizontal well extension capacity," *Fault Block Oil and Gas Field*, vol. 23, no. 5, pp. 643–647, 2016.

[28] G. Bi, G. S. Li, Z. Qu et al., "Rock breaking effect of self-propelled rotary jet drill," *Acta Petrolei Sinica*, vol. 37, no. 5, pp. 680–687, 2016.

[29] G. L. Yang, W. H. Zhou, and F. Liu, "Flow field simulation of high-pressure water jet nozzle based on fluent," *Journal of Lanzhou University of Technology*, vol. 34, no. 2, pp. 49–52, 2008.

[30] G. Z. Wang, C. Y. Ran, B. Deng et al., "Study on jet characteristics of long-distance flushing nozzle based on FLUENT," *Hydraulics Pneumatics & Seals*, vol. 36, no. 1, pp. 31–34, 2016.

[31] D. Y. Zhu, D. Y. Liang, P. W. Shi et al., "Study on the influence of ore jet nozzle structure on jet flow field," *Mineralogy & Metallurgy*, vol. 25, no. 6, pp. 65–69, 2016.

[32] K. Shen, J. Yang, L. Ma et al., "Research and application of hydraulic jet composite plugging removal technology," *Petrochemical Applications*, vol. 30, no. 1, pp. 48–35, 2011.

[33] T. G. Chen, Z. C. Guan et al., *Drilling Engineering Theory and Technology*, China University of Petroleum, Dongying, China, 2006.

[34] H. J. Zhu, Y. H. Lin, and L. H. Xie, *FLUENT Fluid Analysis and Simulation Practical Tutorial*, People's Posts and Telecommunications, Beijing, China, 2010.

[35] C. H. Li and Y. Y. Zhang, "Numerical simulation of mechanical degradation of polymer solution under the shaft," *Value Engineering*, vol. 33, no. 49, pp. 124–126, 2016.

Hindawi
Advances in Polymer Technology
Volume 2020, Article ID 2914375, 7 pages
https://doi.org/10.1155/2020/2914375

Research Article

Study on Wellbore Temperature and Pressure Distribution in Process of Gas Hydrate Mined by Polymer Additive CO_2 Jet

Minghui Wei, Chenghuai Wu, and Yanxi Zhou

College of Mechanical and Electrical Engineering, Southwest Petroleum University, Chengdu, China

Correspondence should be addressed to Minghui Wei; wmh881988@163.com

Received 29 May 2019; Revised 24 July 2019; Accepted 31 July 2019; Published 10 January 2020

Guest Editor: Hou Jian

In order to solve the problem of hydrate reservoir collapse and hydrate regenerated in the process of solid fluidization of natural gas hydrate, a new method of natural gas hydrate exploit by high-polymer additive (low viscosity carboxymethyl cellulose LV-CMC) carbon dioxide jet was proposed. The wellbore temperature and pressure changes during this process are analyzed, and the wellbore temperature and pressure model are established and solved by the state space method. This paper also analyzed the effects of relevant parameters on hydrate decomposition, such as injection flow, temperature, and pressure. The results show that increasing the injection pressure allows the hydrate decomposition site to be closer to the annulus outlet. Compared with water, with polymer additive CO_2 fluid as the drilling fluid, the intersection point of phase equilibrium curve and annular pressure curve is closer to annular outlet, which is obviously more conducive to well control. In order to avoid phase changes, the injection pressure of the carbon dioxide fluid of the high-polymer additive should not be lower than 10 MPa, and the injection temperature should not be higher than 285 K.

1. Introduction

Natural gas hydrate has great potential for future energy resources supply, which has the characteristics of wide distribution, shallow burial, and high energy density. According to the conditions of temperature less than 283 K and the pressure greater than 10 MPa, about 27% of the world's land and 90% of the ocean have the potential for gas hydrate formation generation. The reserves of natural gas hydrates in the world are very large. It is estimated that the natural gas resources in hydrates are $2 \times 10^{16}\ m^3$, which is equivalent to 2×10^5 billion tons of oil equivalent, and twice the total amount of carbon of conventional fuels in the world. Traditional gas hydrate mining methods include heat injection method, decompression method, carbon dioxide replacement method, etc., But these methods have not been widely used because of the problems of wellbore safety, production control, and environmental risk [1–3]. The natural gas hydrate solid fluidized mining method could overcome these problems effectively [4]. The method is to use the jet to break the bottom hole hydrate into fine particles, and the hydrate-containing solid particles after fluidization return along the wellbore to the sea surface with the drilling fluid, and finally separate out the natural gas.

In the natural gas hydrate solid fluidized mining method, the hydrate reservoir is liable to collapse, and the decomposed natural gas hydrate may be regenerated, causing blockage of the wellbore and causing a drilling accident [5]. Carbon dioxide fluid containing LV-CMC as jet drilling fluid can effectively solve these problems, on the one hand, because both carbon dioxide and LV-CMC can inhibit the formation of natural gas hydrate; on the other hand, LV-CMC, as a drilling fluid additive, also plays a role in reducing leakage and preventing collapse. In addition, in order to prevent the jet viscosity from being too large and affecting the jet efficiency, we use a jet drilling fluid with an additive concentration of 5%. And when the concentration of the polymer additive is 5%, the physical properties of the carbon dioxide fluid are not greatly affected [6].

Carbon capture and storage (CCS) is a technology that can reduce carbon emissions from fossil fuels on a large scale [7]. The technology was developed in the 1970s for oil, geothermal and other energy development, as well as water treatment and other technologies [8–15]. In the process of extracting natural gas hydrates using high-polymer additive carbon dioxide jet, correct prediction of wellbore temperature and pressure is of great significance for judging the properties of polymer additive CO_2 fluid and analyzing the state of

natural gas hydrate. However, there is very little research work in this field.

Since 1950s, drilling workers have begun to study the temperature distribution of wellbore by numerical simulation and analytical method [15]. The earliest wellbore temperature study was conducted by Ramey, who proposed a steady-state model for obtaining wellbore temperature distribution, which could not be applied to transient behavior [16–19]. Raymond proposed a numerical model for wellbore temperature distribution under pseudo-steady-state conditions [20]. Hansan and Kabir proposed an analytical method for wellbore temperature prediction [21, 22]. For CO_2 injection drilling and development methods, wellbore flow and thermal behavior have unique characteristics. Many researchers also developed CO_2 two-phase flow models under isothermal conditions [23–24]. However, the process of natural gas hydrate exploitation is different from injecting polymer additive CO_2 fluid into wellbore. It also needs to consider the heat transfer of annular, pipeline, seawater, and hydrate decomposition, but this field has not been studied for the time being.

In this paper, the mathematical model of wellbore temperature and pressure during polymer additive CO_2 fluid injection is established, and the model is solved by state space method. This method can be used not only to solve partial differential equations, but also as an automatic control model, which lays a foundation for automatic control of temperature and pressure in natural gas hydrate mining process in the future. This study can be used to design the injection parameters of polymer additive CO_2 fluid and reduce the risk of using this drilling fluid to extract natural gas hydrate.

2. Materials and Methods

Low viscosity carboxymethyl cellulose (LV-CMC) is a polymer. Hydroxyl OH and ether oxygen group on the macromolecular chain are absorbed to the surface of the hydrate crystal. The polymer forces the hydrate crystal to grow around the polymer with a small radius of curvature, thus reducing the rate of hydrate formation and prolonging the time of hydrate crystal nucleus formation. In view of the fact that fluidized natural gas hydrates may be formed again during deep-water oil and gas drilling, we chose carbon dioxide fluid with LV-CMC as jet drilling fluid.

The change of phase state of CO_2 at certain temperature and pressure will lead to change in the properties of carbon dioxide. Figure 1 describes phase change of CO_2, when CO_2 approaches the supercritical state (31.1°C, 7.38 MPa), which is likely to occur somewhere along the wellbore.

2.1. Thermodynamic Properties. In 1996, Span and Wagne [26] proposed a special equation of state for carbon dioxide (hereinafter referred to as the S-W equation). It can be applied to a wide range of applications (216.59 K < T < 1100 K, 0.52 MPa < p < 800 MPa) with high accuracy. Therefore, it is more suitable to calculate the thermodynamic properties of polymer additive carbon dioxide fluid under high temperature and high pressure.

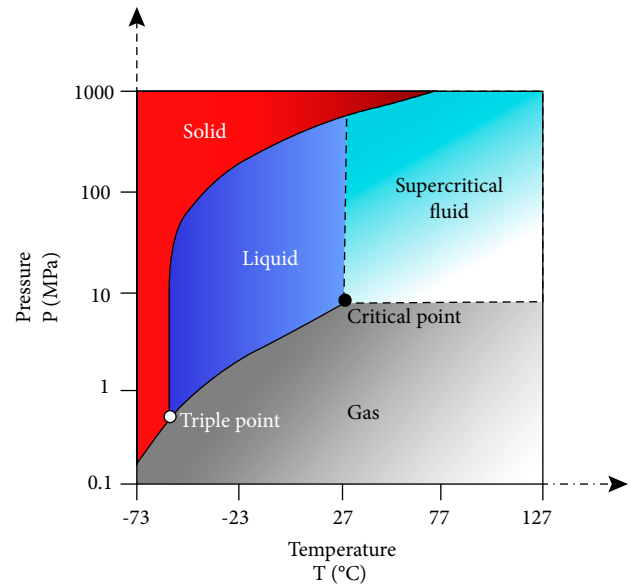

Figure 1: Phase change of carbon dioxide.

The S-W equation is expressed in the form of Helmholtz free energy with two independent variable temperatures T and density ρ. The dimensionless Helmholtz free energy $\Phi(\delta, \tau)$ can be divided into the ideal gas part $\Phi^0(\delta, \tau)$ and the residual fluid part$\Phi^t(\delta, \tau)$, namely:

$$\Phi(\delta, \tau) = \Phi^0(\delta, \tau) + \Phi^t(\delta, \tau) \tag{1}$$

here $\delta = \rho_c/\rho$, $\tau = T_c/T$, dimensionless.

According to the S-W formula and proportion of additive (5%), the solution of the density, isostatic heat capacity, Joule-Thomson coefficient and other thermodynamic properties of the polymer additive CO_2 fluid can be obtained.

2.2. Heat Transfer Model. Figure 2 describes the process of injecting the polymer additive CO_2 fluid for natural gas hydrate exploitation. The process can be divided into three parts. The first, the polymer additive CO_2 fluid is injected into the coiled tubing. The second, the fluids flow through the jet bit and flow into the annulus. The third, the fluids flow through the annulus and to the sea surface.

Based on the principle of conservation of energy, we can establish the dynamic mathematical model of heat transfer in the process of injecting the polymer additive CO_2 fluid:

2.2.1. The heat transfer model of tubing fluids. For the polymer additive CO_2 fluid in the tubing, the energy change is equal to the heat generated by the axial flow of the fluid, the heat exchange between the fluid in the tubing and the fluid in the annulus, and the heat generated by the pressure change. Therefore, the heat transfer model is:

$$\begin{aligned}\rho_b A_p C_p \frac{\partial T_p}{\partial t} &= -M_p C_p \frac{\partial T_p}{\partial z} + 2\pi r_1 \lambda_{12}\left[T_w - T_p\right] \\ &\quad + \alpha_p M_p C_p \frac{\partial p_p}{\partial z},\end{aligned} \tag{2}$$

where ρ_b is the density of tubing fluid, kg/m^3, A_p is the area of the tubing, m, T_p is the temperature of the fluid in the tubing,

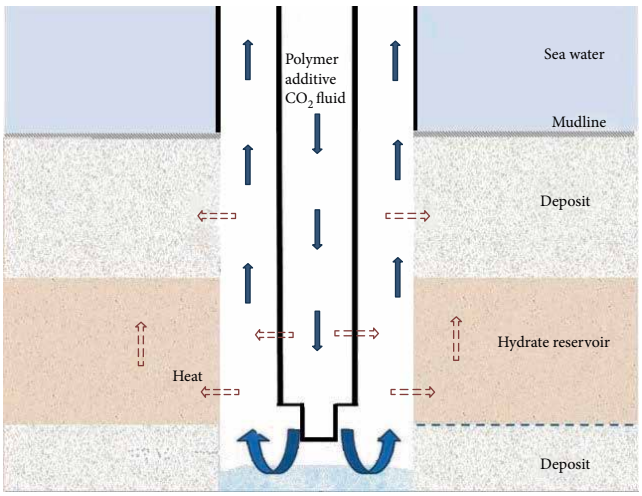

Figure 2: Schematic diagram of polymer additive CO_2 fluid injection process.

K, T_w is the temperature of the tubing, K, p_p is the pressure of the fluid in the tubing, MPa, C_p is the specific heat of tubing fluids, J/kg·K, r_1 is the inner radius of tubing, m, v_p is the fluids flow velocity in the tubing, m/s, λ_{12} is the convective heat transfer coefficient between tubing the polymer additive CO_2 fluids and tubing, W/m^2·K, and α_p is Joule-Thomson coefficient, K/MPa.

2.2.2. The heat transfer model of annulus. According to Figure 2, we can know the heat transfer model of the polymer additive CO_2 fluid in the annulus. The energy change is equal to the heat generated by the axial flow of the fluid, the heat transfer between the annulus fluid and the pipeline fluid, and the heat transfer between the wellbore fluid and the annulus fluid. Therefore, the heat transfer model is:

$$\begin{aligned}\rho_a A_a C_a \frac{\partial T_a}{\partial t} &= -M_a C_a \frac{\partial T_a}{\partial z} + 2\pi r_2 \lambda_2 [T_w - T_a] \\ &\quad + 2\pi r_3 \lambda_3 [T_f - T_a] + \alpha_a M_a C_a \frac{\partial p_a}{\partial z},\end{aligned} \tag{3}$$

where ρ_a is the polymer additive CO_2 fluid density of annulus, kg/m^3, A_a is the area of annulus, m^2, T_a is the temperature of the fluid in the annulus, K, T_w is the temperature of the tubing, K, p_a is the pressure of the fluid in the annulus, MPa, C_a is the polymer additive CO_2 fluid specific heat of annulus fluid, J/kg·K, M_a is the mass flow of injected polymer additive CO_2 fluid, kg/s, r_2 is the outer radius of tubing, m, r_3 is the radius of annulus, m, λ_{21} is the convection heat transfer coefficient of annular fluid and tubing, λ_3 is the convection heat transfer coefficient of annular fluid and borehole wall, W/m^2·°C, α_a is the Joule-Thomson coefficient, K/MPa.

2.2.3. The heat transfer model of tubing. For the tubing, the change of energy is equal to the convection heat transfer between the annulus fluids and tubing, and the convection heat transfer between the tubing fluids and tubing. Therefore, the heat transfer model is:

$$\rho_w A_w C_w \frac{\partial T_w}{\partial t} = 2\pi r_2 \lambda_{21} [T_a - T_w] + 2\pi r_1 \lambda_{12} [T_p - T_w], \tag{4}$$

where ρ_w is the density of tubing, kg/m^3, A_w is the area of tubing, m^2, and C_w is the specific heat of tubing, J/kg·K.

2.3. Wellbore Pressure Model. According to the mass conservation equation and momentum equation, we can get the wellbore pressure model:

$$\frac{\partial}{\partial z}(p_a v_a) = 0 \tag{5}$$

$$\frac{\partial}{\partial z}\left(p_a {v_a}^2\right) = -\frac{\partial p_a}{\partial z} + \rho_a g \sin\theta - \frac{\tau_w \pi d}{A_p}. \tag{6}$$

Substituting the mass conservation equation into the momentum equation and replacing the friction term of wall, flowing pressure equation of the polymer additive CO_2 fluid flow downward in the tubing can be deduced

$$\frac{\partial p_a}{\partial z} = -\rho_a g \frac{\partial v_a}{\partial z} + \rho_a g \sin\theta - f \frac{\rho v_a^2}{2d}, \tag{7}$$

where f is Darcy friction factor and v_a is annulus flow rate, m/s.

2.4. Hydrates Phase Equilibrium Model. According to Dzyuba's natural gas hydrate phase equilibrium model [4], the relationship between temperature and pressure is:

$$p_E = \frac{T_a - 264.9661}{9.6339}, \tag{8}$$

where p_E is hydrate phase equilibrium pressure at the temperature T_a, MPa.

2.5. State-Space Method for the Wellbore. For Equation (4), using difference instead of integral, therefore:

$$\begin{aligned}\frac{\partial T}{\partial t} &= \frac{T(k+1,1) - T(k,1)}{\Delta t}, \\ \frac{\partial T}{\partial z} &= \frac{T(1,j) - T(1,j-1)}{\Delta z}.\end{aligned} \tag{9}$$

Equation (2) can be expressed as:

$$\begin{aligned}\rho_a A_a C_a \frac{T_a(k+1,j) - T_a(k,j)}{\Delta t} &= -M_a C_a \frac{T_a(k,j) - T_a(k,j-1)}{\Delta z} \\ &\quad + 2\pi r_2 \lambda_2 [T_w(k,j) - T_a(k,j)] \\ &\quad + 2\pi r_3 \lambda_3 [T_f(k,j) - T_a(k,j)] \\ &\quad + \alpha_a M_a C_a \frac{\partial p_a}{\partial z}.\end{aligned} \tag{10}$$

The depth of wellbore is divided into L nodes, according to linear system theory, each grid temperature in the tubing and annulus is a state. We set the gas injection temperature as $T_a(k,0)$, and set $x_1 = -(M_a \Delta t)/(\rho_a A_a \Delta z)$, $x_2 = 2\pi r_2 \lambda_2 \Delta t/(\rho_a A_a C_a)$, $x_3 = 2\pi r_3 \lambda_3 \Delta t/(\rho_a A_a C_a)$, $Q = \alpha_a M_a C_a (\partial p_a)/(\partial z)$, the state-space model for wellbore heat transfer system can be represented as:

$$T_A(k+1) = A_a T_A(k) + B_a T_w(k) + C_a T_f(k) + D_a U_d(k), \tag{11}$$

where,

$$T_A(k) = \left[T_a(k,1), T_a(k,2), T_a(k,3), \cdots T_a(k,L)\right]^T_{L\times 1} \tag{12}$$

$$T_w(k) = \left[T_w(k,1), T_w(k,2), T_w(k,3), \cdots T_w(k,L)\right]^T_{L\times 1} \tag{13}$$

$$T_f(k) = \left[T_f(k,1), T_f(k,2), T_f(k,3), \cdots T_f(k,L)\right]^T_{L\times 1} \tag{14}$$

$$U_d(k) = \left[T_a(k,0), Q, 0, \cdots 0\right]^T_{L\times 1} \tag{15}$$

$$A_a = \begin{bmatrix} x_1+1-x_2-x_3 & 0 & 0 & \cdots & 0 \\ -x_1 & x_1+1-x_2-x_3 & 0 & \cdots & 0 \\ 0 & -x_1 & \ddots & \ddots & 0 \\ \vdots & 0 & \ddots & x_1+1-x_2-x_3 & 0 \\ 0 & 0 & 0 & -x_1 & x_1+1-x_2-x_3 \end{bmatrix}_{L\times L}, \tag{16}$$

$$B_a = x_2,$$
$$C_a = x_3,$$
$$D_a = -x_1,$$

T_A is the state vector of wellbore heat transfer state-space model, U_d is the input vector, and A_a is the system matrix. In the same way, we can get the state space model of the fluid temperature in the tubing.

$$T_P(k+1) = A_p T_P(k) + B_p T_w(k) + D_p U_p(k). \tag{17}$$

In this process, the heat sources are the seawater temperature, the formation temperature and the hydrate reservoir temperature, according to literature [4], we can calculate the seawater temperature

$$T_s = \frac{1}{200}\left[(T_{s0} - 273.15)(200 - z) + 13.7h\right], \quad 0 \le z < 200\,m$$
$$T_s = a_1 - \frac{a_1 - a_2}{1 + e^{z + a_3/a_4}}, \quad z \ge 200\,m, \tag{18}$$

where T_s represents the temperature of seawater, K; T_{s0} represents the temperature of sea surface, K; z represents the depth of seawater, m; a_1, a_2, a_3, a_4 represent curve fitting coefficients, respectively.

3. Results

In order to verify this model, we do simulation to get the distribution of wellbore temperature and pressure and the location of gas hydrate decomposition point under different conditions. The basic data of the simulation derived from literature [4, 23], and are shown in Table 1.

3.1. The Influence of Injection Rate. When the injection rates of the polymer additive CO_2 fluid are 40 L/min, 60 L/min, 80 L/min, and 100 L/min, using this model, the annulus temperature and pressure can be obtained.

Figure 3 shows the temperature distribution of annulus under different polymer additive CO_2 fluid injection rates. The larger the drilling fluid flow rate, the shorter the heat exchange time between the annulus and the seawater, and the less the temperature of annulus is affected by seawater.

Figure 4 shows that annulus pressure decreases as the flow rate increases. For the upper section of wellbore, the phase equilibrium pressure decreases as the flow rate increases, for the lower section of wellbore, the phase equilibrium pressure changes almost unchanged with the change of flow rate. The intersection of annulus pressure and phase equilibrium pressure curve moves upward (The intersection point refers to the critical decomposition position of the natural gas hydrate); this is contrary to the conclusion in [4]. Under this condition of injection temperature and pressure, the decomposition position of hydrate is between depth 150 and 200 m.

During the actual drilling process, phase changes of the polymer additive CO_2 fluid are not expected. According to Figures 4 and 5, the minimum pressure and maximum temperature of the polymer additive CO_2 fluid are at the annulus outlet. The temperature and the pressure corresponding to the different flow rates are shown in Table 2. According to the S-W equation, there is no phase change during this process. In practice, in order to ensure operation safely, the injection pressure should be increased and the injection temperature should be reduced as possible.

3.2. The Influence of Injection Temperature. Figure 5 shows the annulus pressure and phase equilibrium curves under different injection temperatures, when the flow rate is 100 L/min. Due to the injection temperature increase, the phase equilibrium pressure increases, and the annulus pressure increases a little. The injection temperature effects on the depth of decomposition point very little.

Table 1: Calculation parameters.

Parameter	Value	Parameter	Value
Well depth/m	1200	Mass flow rate/ (L/min)	40
Coiled Tubing inner diameter/mm	40	Injection pressure/ MPa	25
Coiled Tubing outer diameter/mm	51	Injection temperature/°C	21
Drilling string inner diameter/mm	114	Surface earth temperature/°C	20
Drilling string outer diameter/mm	127	Fluids density/ (kg/m3)	1040

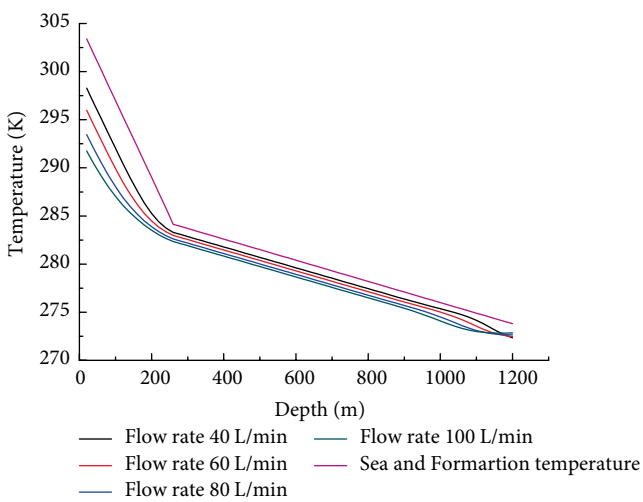

Figure 3: The annulus temperature distribution with different injection rate.

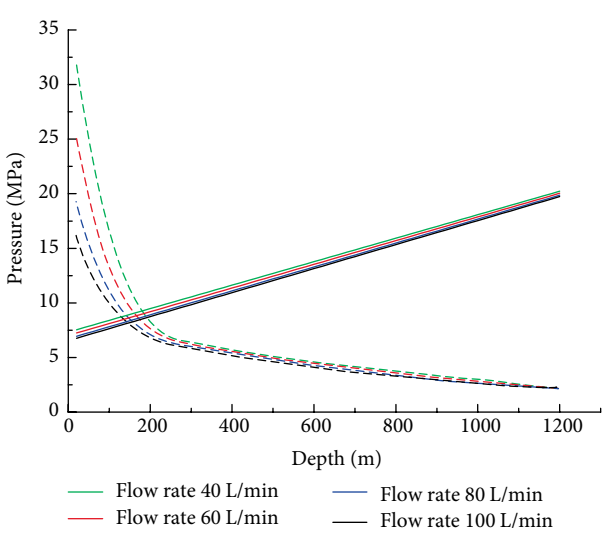

Figure 4: The annulus pressure distribution and hydrates phase equilibrium with different injection rates.

3.3. Comparison With Water. In order to compare the difference between using polymer additive CO_2 fluid and using water as drilling fluid, we do the simulation. As in practice,

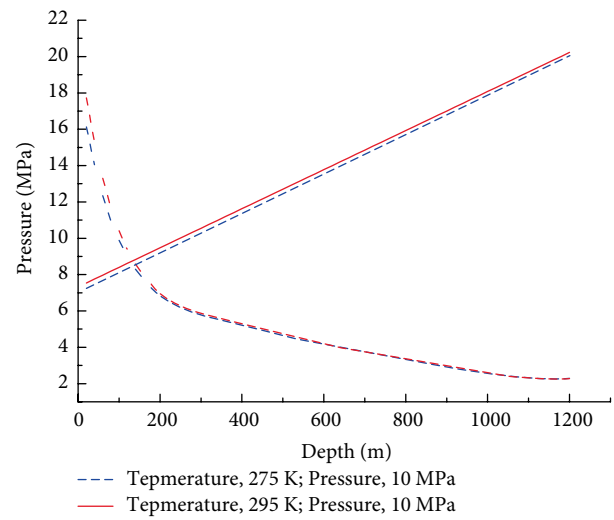

Figure 5: The annulus pressure distribution and hydrate phase equilibrium with different injection temperatures.

Table 2: Flow rate-pressure/temperature.

Flow rate, L/min	Pressure, MPa/Temperature, K
40	7.54/298.27
60	7.24/295.99
80	6.94/293.45
100	6.76/291.75

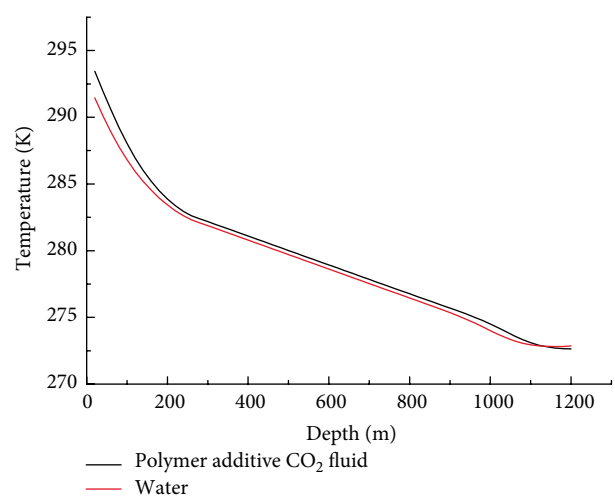

Figure 6: The annulus temperature distribution comparison between the polymer additive CO_2 fluid and water as drilling fluids.

water is difficult to achieve low temperature as a drilling fluid, the injection water temperature is set at 285 K, the injection pressure is 10 MPa, and the injection amount is 10 L/min. The polymer additive CO_2 fluid injection temperature is 275 K, and other conditions keep the same.

Figure 6 shows the annulus temperature distribution. Since the specific heat of the polymer additive CO_2 fluid is less than the specific heat of the water, it is greatly affected by the seawater

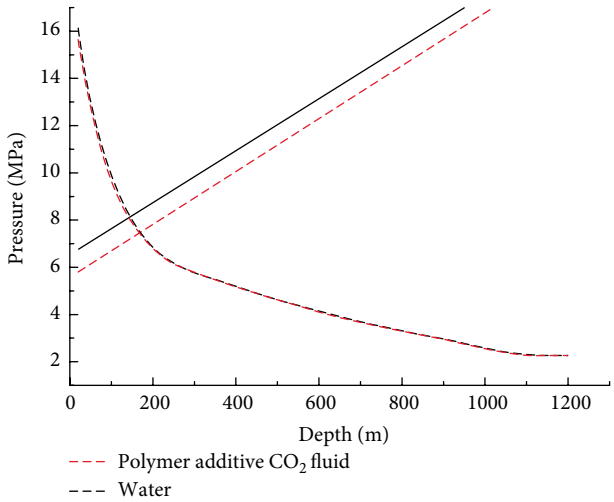

Figure 7: The annulus pressure distribution and hydrates phase equilibrium comparison between the polymer additive CO_2 and water as drilling fluids.

temperature. Figure 7 shows the relationship between the annulus pressure and the phase equilibrium pressure. The equilibrium curves of the two are almost coincident. When polymer additive CO_2 fluid is used as the drilling fluid, the decomposition position of the hydrate is closer to the wellhead.

4. Conclusions

Based on the above study, we can draw the following conclusions:

(1) Increasing the pressure of injection can get the hydrate decomposition position closer to the annulus outlet.

(2) Compared with water, using polymer additive CO_2 fluids as drilling fluids, the intersection of phase equilibrium curve and the annulus pressure curve is closer to the annulus outlet, which is obviously beneficial to the implementation of well control.

(3) However, due to the special properties of the polymer additive CO_2 fluid, in order to ensure that the polymer additive CO_2 fluids do not result in a phase change during the drilling process, it is necessary to increase the pressure and reduce the temperature of the injection CO_2; this is very difficult for the equipment. According to the calculation, it is suggested that the injection pressure should not be lower than 10 MPa and the injection temperature should not be higher than 285 K.

(4) When the polymer additive CO_2 fluid is used as the drilling fluid, the intersection of the phase equilibrium curve and the annulus pressure curve increases as flow rate increases, which is contrary to the conclusion in [4]. The reason is the focus of future research.

Data Availability

All data included in this study are available upon request by contact with the corresponding author.

Conflicts of Interest

The authors declare that there is no conflict of interest regarding the publication of this paper.

Acknowledgments

This research was funded by State Key Laboratory of Petroleum Resources and Prospecting, China University of Petroleum, Beijing, grant number PRP/open-1610 and National Natural Science Foundation of China, grant number 51804267.

References

[1] R. C. Zheng, S. H. B. Yang, P. Babu, P. Linga, and X.-S. Li, "Review of natural gas hydrates as an energy resource: prospects and challenges," *Applied Energy*, vol. 162, pp. 1633–1652, 2016.

[2] R. Boswell and T. S. Collett, "Current perspectives on gas hydrate resources," *Energy & Environmental Science*, vol. 4, no. 4, pp. 1206–1215, 2011.

[3] X.-S. Li, B. Yang, Y. Zhang et al., "Experimental investigation into gas production from methane hydrate in sediment by depressurization in a novel pilot-scale hydrate simulator," *Applied Energy*, vol. 93, no. 6, pp. 722–732, 2012.

[4] S. Zhou, Q. Li, W. Chen et al., "The world's first successful implementation of solid fluidization well testing and production for non-diagenetic natural gas hydrate buried in shallow layer in deep water," vol. 4, in *Proceedings of the Annual Offshore Technology Conference*, pp. 2784–2794, Houston, TX, USA, 2018.

[5] L. Zeng, J. Ding, and J. Xu, "Study on a kind of effective compound inhibitor of gas hydrate," *Guangdong Chemical Industry*, vol. 35, no. 3, pp. 8–10, 2008.

[6] B. J. Sun, X. L. Liu, and S. R. Ren, "Experiment on inhibition of drilling fluid additives for natural gas hydrate formation," *Journal of China university of petroleum (Natural Science Edition)*, vol. 32, no. 1, pp. 56–59, 2008.

[7] Z. Chen, X. Liao, X. Zhao, X. Dou, and L. Zhu, "Development of a trilinear-flow model for carbon sequestration in depleted shale," *SPE Journal*, vol. 21, no. 4, pp. 1386–1399, 2016.

[8] T. A. Buscheck, Y. Sun, Y. Hao et al., "Combining brine extraction, desalination, and residual-brine reinjection with CO_2 storage in saline formations: implications for pressure management, capacity, and risk mitigation, Amsterdam Netherlands," *Energy Procedia*, vol. 4, pp. 4283–4290, 2011.

[9] X. Huang, T. Li, H. Gao, J. Zhao, and C. Wang, "Comparison of SO_2 with CO_2 for enhancing shale-hydrocarbon recovery using low-field nuclear magnetic resonance," *Fuel*, vol. 245, pp. 563–569, 2019.

[10] Q. Li, Y. N. Wei, G. Liu, and Q. Liu, "Combination of CO_2 geological storage with deep saline water recovery in western China: insights from numerical analyses," *Applied Energy*, vol. 116, pp. 101–110, 2014.

[11] H. Wang, G. Li, and Z. Shen, "A feasibility analysis on shale gas exploitation with supercritical carbon dioxide," *Energy Sources, Part A: Recovery, Utilization, and Environmental Effects*, vol. 34, no. 15, pp. 1426–1435, 2012.

[12] F. Luo, R.-N. Xu, and P.-X. Jiang, "Numerical investigation of the doublet enhanced geothermal system with CO_2 as working fluid (CO_2-EGS)," *Energy*, vol. 64, pp. 307–322, 2014.

[13] M. Boot-Handford, J. C. Abanades, E. Anthony et al., "Carbon capture and storage update," *Energy Environment Science*, vol. 7, no. 1, pp. 130–189, 2014.

[14] R. S. Middleton, J. W. Carey, R. P. Currier et al., "Shale gas and non-aqueous fracturing fluids: opportunities and challenges for supercritical CO_2," *Applied Energy*, vol. 14, no. 7, pp. 500–509, 2015.

[15] H. Sun, J. Yao, S.-H. Gao, D.-Y. Fan, C.-C. Wang, and Z.-X. Sun, "Numerical study of CO_2 enhanced natural gas recovery and sequestration in shale gas reservoirs," *International Journal of Greenhouse Gas Control*, vol. 19, pp. 406–419, 2013.

[16] A. R. Hasan and C. S. Kabir, "A mechanistic model for computing fluid temperature profiles in gas-lift wells," *SPE Production and Facilities*, vol. 11, no. 3, pp. 179–185, 1996.

[17] H. J. Ramey, "Wellbore heat transmission," *Journal of Petroleum Technology*, vol. 14, no. 4, pp. 427–435, 1962.

[18] M. Yang, X. Zhao, Y. Meng et al., "Determination of transient temperature distribution inside a wellbore considering drill string assembly and casing program," *Applied Thermal Engineering*, vol. 118, pp. 299–314, 2017.

[19] A. R. Hasan and C. S. Kabir, *Fluid Flow and Heat Transfer in Wellbores*, SPE Richardson, Texas, 2002.

[20] L. R. Raymond, "Temperature distribution in a circulating drilling fluid," *Journal of Petroleum Technology*, vol. 21, no. 3, pp. 333–341, 1969.

[21] A. R. Hasan, C. S. Kabir, and X. Wang, "Development and application of a wellbore/reservoir simulator for testing oil wells," *SPE Formation Evaluation*, vol. 12, no. 3, pp. 182–190, 1997.

[22] A. R. Hasan, C. S. Kabir, and X. Wang, "Wellbore two-phase flow and heat transfer during transient testing," *SPE Journal*, vol. 3, no. 2, pp. 174–182, 1998.

[23] H. Wang, Z. Shen, and G. Li, "Influences of formation water invasion on the wellbore temperature and pressure in supercritical CO_2 drilling," *Petroleum Exploration Development*, vol. 38, no. 3, pp. 362–368, 2011.

[24] X. Li, G. Li, H. Wang et al., "A coupled model for predicting flowing temperature and pressure distribution in drilling ultra-short radius radial wells," in *IADC/SPE Asia Pacific Drilling Technology Conference*, Singapore, August 22–24, 2016.

[25] J. Guo and J. Zeng, "A coupling model for wellbore transient temperature and pressure of fracturing with supercritical carbon dioxide," *Shi You Xue Bao/ActaPet. Sin*, vol. 36, no. 2, pp. 203–209, 2015.

[26] R. Span and W. Wagner, "A new equation of state for carbon dioxide covering the fluid region from the triple-toint temperature to 1100 K at pressures up to 800 MPa," *Journal of Physical and Chemical Reference Data*, vol. 25, no. 6, pp. 1509–1596, 1996.

[27] Z. M. Wang, X. N. Hao, X. Q. Wang, L. Xue, and X. L. Guo, "Numerical simulation on deep water drilling wellbore temperature and pressure distribution," *Petroleum Science and Technology*, vol. 28, no. 9, pp. 911–919, 2010.